Preliminary slip rate estimates for the Düzce segment of the North Anatolian Fault Zone from offset geomorphic markers

S. Pucci [(1 and 2) *], P.M. De Martini [(1)] and D. Pantosti [(1)]

(1) Sismologia e Tettonofisica, Istituto Nazionale di Geofisica e Vulcanologia, via di Vigna Murata, 605, 00143 Roma, Italy

(2) Dipartimento di Scienze della Terra, Universita' degli Studi di Perugia, piazza dell'Università, 06128 Perugia, Italy

*Corresponding Author, pucci@ingv.it

Keywords: tectonic geomorphology, geomorphic markers, slip rate, strike-slip, 1999 Düzce earthquake.

Abstract

New punctual estimates on the Quaternary slip rate of the active transform margin of North Anatolia are provided.

We investigated the area struck by the 12 November 1999, Mw 7.1 earthquake, that ruptured the Düzce fault segment of the North Anatolian Fault. In order to analyze the spectacular tectonically driven cumulative landforms and the drainage pattern settings, we carried out a 1:25,000-scale geological and geomorphological mapping along the fault trace. We reconstruct and describe, as offset geomorphic markers, right-hand stream deflections and fluvial terraces inset into alluvial fan deposits. Radiocarbon dating indicates that ~100 m stream deflections were built up by the last ~7000 yr BP fault activity. Conversely, two documented and correlated Late Pleistocene fluvial terraces are horizontally offset by ~300 and ~900 m, respectively. These were dated by means of Optically Stimulated Luminescence (OSL) method to ~21 ka BP and 60 ka BP. Assuming a constant rate of deformation for the Düzce Fault, ages and related offsets translate to consistent slip-rates that yield an average slip-rate of 15.0 ± 3.2 mm/yr for the last 60 ka.

Thus, the Düzce Fault importantly contributes to the North Anatolian margin deformation, suggesting a present-day partitioning of displacement rates with the Mudurnu fault to the south and confirming its relevant role in the seismic hazard of the area.

1. Introduction

Along the active transform margin of North Anatolia, the outstanding morphology of strike slip faulting is one of the direct consequences of long-lasting deformation (Fig. 1a). However, limited documented offset of structural or geomorphic markers exist along the 1500 km-long North Anatolian Fault Zone (NAFZ) (Dhont et al., 1998; Armijo et al., 1999; Hubert-Ferrari et al., 2002; Polonia et al., 2004; Şengör et al., 2005) (Fig. 1b). Thus, there is still need for detailed case studies to better constrain the geological slip rates and to increase the understanding of the NAFZ activity on both temporal and spatial scales.

With this aim, we investigated the area struck by a Mw 7.1 earthquake, on November 12th 1999, that ruptured the Düzce segment. This area is favorable for slip rate studies because of (1) extensive faulted Pleistocene and Holocene continental deposits, (2) high preservation potential of the landforms with respect to the time scale of the tectonic process, and (3) deformation recorded and localized in the landscape close to the surface expression of the fault as recognized following the 1999 earthquake (Pucci et al., 2006 and Pucci, 2007).

In this work we present new measurements of cumulative fault-related offset of geomorphic markers, useful for preliminary Düzce fault slip rate estimates over different time periods. We applied methodologies used in similar tectonically active regions (*e.g.* California, New Zealand), where the recognition of lateral displacements of streams and alluvial terraces, resulting from active strike-slip faulting (Wallace, 1968; Huang, 1993; Jackson et al., 1996; Burbank and Anderson, 2001), were combined with

age controls (e.g., Matsuda, 1967; Keller et al., 1982; Sieh and Jahns, 1984; Van Dissen and Berryman, 1996).

In the following, after a brief introduction on the tectonic framework of the NAFZ and on the Düzce fault segment, we describe the measured offset geomorphic markers and their dating and in particular: (1) alluvial terraces and related deflected streams; (2) fluvial terraces inset in old alluvial fans.

In order to understand whether changes in the fault motion occurred in space and time or both, we compared the obtained slip rates at different time-scale.

2. The North Anatolian Fault Zone (NAFZ)

The NAFZ is an active right-lateral system, about 1500 km long, which bounds the westward-extruding Anatolian block to the north (McKenzie, 1972; Şengör, 1979; Barka, 1992; Şaroğlu et al., 1992) (Fig. 1a) that, based on the age of fault-related basin deposits, is considered active since Late Miocene (Şengör et al., 1985; Dewey et al., 1986; Şengör et al., 2005) or Early Pliocene (Barka, 1992). To the east of the town of Bolu, the NAFZ is formed by a main single trace but, west of it, it splays into two main strands, the Düzce and the Mudurnu fault segments (Fig. 1b). Farther west, it splays again into three major strands that formed the pull-apart basins hosting the Marmara Sea (Wong et al., 1995; Le Pichon et al., 2001; Armijo et al., 1999; Okay et al., 1999).

Seismicity along the NAFZ is characterized by frequent moderate to large earthquakes (M>7) with focal mechanism solutions that show

essentially pure right-lateral strike-slip motion (Canitez and Ucer, 1967; McKenzie, 1972; Reinecker et al., 2004). The number of large historical earthquakes occurred along the NAFZ during the last centuries places this fault among the most active strike-slip structures worldwide (Ambraseys, 1970; Ambraseys and Finkel, 1995; Ambraseys, 2002). Seismic moment release over the past 100-400 years suggests deformation rates of 20 ± 10 mm/yr (Jackson and McKenzie, 1988; Westaway, 1994).

Regional GPS networks indicate fault-parallel vectors with strain-rates in the northern part of the Anatolian block up to 25 ± 5 mm/yr (Reilinger et al., 1997 and 2000; Straub et al., 1997; McClusky et al., 2000; Kahle et al., 1999 and 2000) (Fig. 1).

The slip-rates documented from geology and geomorphology along the NAFZ show a limited spatial distribution, and most of them are calculated on Plio-Pleistocene markers (a summary is reported in Fig. 1b). These slip rates show a large variability (from 2 mm/yr up to 24 mm/yr) and present large uncertainties or are much smaller than the present-day geodetic measurements. This suggests an acceleration of the deformation over time or an understimation in measuring and dating geological offsets.

2.1 The Düzce fault segment of the NAFZ

The Düzce fault segment has an average E-W trend and a clear geomorphic expression for about 40 km. It separates the Paleozoic-Eocene formations of the Almacik block from the Quaternary continental deposits of the Düzce basin (Fig. 2). Although with internal differences, the overall long-term morphological expression of the Düzce fault depicts a single and

continue structural element that produces relative uplift of the range to the south, with respect to the plain to the north.

According to Ayhan et al. (1999 and 2001), the Düzce Fault accommodates up to 10 mm/yr (*i.e.* 33% to 50% of the net present-day GPS strain of this part of the NAFZ). No slip rates from offset geologic or geomorphic markers exist for the Düzce and Mudurnu faults. Conversely, average slip rates, derived from paleoseismological studies, are of ~10-12.5 mm/yr for the past 2000yrs for the Düzce fault (Pucci, 2007) and 11 ± 5 mm/yr for the Mudurnu fault (Ikeda et al., 1991; Yoshioka et al., 1991).

The most recent coseismic rupture along the Düzce Fault occurred on 12 November 1999 (Mw 7.1, USGS, KOERI), producing right-lateral surface faulting for a total length of ~40 km with a mean dextral and vertical offsets of 2.7 and 0.9 m, respectively, and a 5.0 m dextral and 2.5 m vertical maxima (Akyuz et al., 2000 and 2002; Pucci, 2007).

3. The overall fault geomorphology

Geological and geomorphological mapping along the 1999 rupture zone at a scale of 1:25,000 was carried out (Fig. 2). The observations were made on 1:18 000 and 1:35 000 scale aerial photographs, 20-m-resolution Digital Elevation Model (interpolated from 1:25 000-scale topography, 10 m digital contours), and standard morphometric derivatives (hill-shaded and slope angle maps), all supported by field survey.

Particular attention was paid to the drainage pattern and to the depositional and tectonic landform analysis. In order to detect suitable sediments for dating, recent continental deposits were investigated in detail. The geological and geomorphological map of the Düzce Fault shows

landforms of the Almacik range-front that were shaped by both erosional/depositional processes and active tectonics.

The erosion of the Almacik block generates sediments for delivery to the Düzce Basin. The alluvial fans at the foot of the range-front merge into coalescent aprons (hereinafter referred as bajadas) composed of Late Pliocene-Late Pleistocene conglomerate-sandstone (zone x, Fig. 2) (Herece and Akay, 2003). Holocene alluvial fans are deposited in subsequent incisions of the old bajadas. All the alluvial fan deposits, generally loose and soft, record continuous landform modification due to faulting and exhibit well-expressed tectonic-related morphologies. As observed for other well known seismogenic structures (*e.g.*, Landers (Sieh et al., 1993; Jhonson et al., 1994; Lazarte et al., 1994); Dast-e Bayaz (Tchalenko and Ambraseys, 1970; Tchalenko and Barberian 1975)), tectonic landforms result to be the surface expression of a localized slip plane at depth. Along the Düzce Fault, such tectonic landforms also reflect a small vertical component of deformation, resulting from strike-slip movement along a non rectilinear fault plane that produces transtension at releasing bends (e.g. spots z, Fig. 2) and transpression at restraining bends (e.g. spots q, Fig. 2).

Along the western section of the Düzce fault, the rupture follows a saw-tooth trajectory. Here, along the range-front foot, linear escarpments, dissected by strong incisions at the stream outlets, along with suspended terraces (spots k, Fig. 2) suggest an important subsidence north of the Düzce Fault.

Conversely, the eastern section of the Düzce Fault (Fig. 2) presents a localized deformation with an E-W trace parallel to the mean trend of the whole Düzce fault. In general, this eastern section of the Düzce Fault

denotes an almost pure strike-slip, right-lateral, kinematics. This section crosscuts both recent continental deposits and bedrock and is associated with well developed landforms indicating its persistent long-term activity. It is characterized by shutter ridges, 300 to 1000 m-long, up to 120 m high (e.g. spots r, Fig. 2), with elongated shapes and long axes paralleling the escarpment. In many cases, the ridges act as natural dams for northward flowing drainages, being thus responsible for the formation of ponds and trapping of Holocene fans against the scarp (e.g. spots t, Fig. 2).

4. The geomorphic markers

In the following we discuss our observations on displaced geomorphic markers investigated along the eastern section of the Düzce Fault. Here, the fault section presents a localized and rectilinear deformation zone (Fig. 2), favorable to gauge deformation through time. We identified deflected drainage pattern at the Tilki-Cicubey area (area A in Fig. 2) and offset river terraces at the Beykoy-Degirmenbası area (area B in Fig. 2). For these features, it was possible to hypothesize a probable initial undeformed geometry and to find recent deposits suitable for dating.

The genesis of these geomorphic markers is strictly related to the evolution of the drainage system of the area. The drainage system is certainly the most sensitive factor to tectonic deformation. However, even in fast tectonically deforming regions, climate may play a dominant role in the production, transport, deposition and erosion of detritus from uplands into a sedimentary basin. The upper reaches of drainage networks are the most sensitive to climate changes, controlling the sediment delivery ratios (Sugai, 1993; Blum and Törnqvist, 2000 and references therein). At the stream

outlet, fan processes are able to operate independently of other extrinsic variables, notably style or rate of tectonics, source-area lithology and geomorphology, and base-level history (*e.g.* Ritter et al., 2000). This was well documented for the late Quaternary in the Mediterranean region (*e.g.* Macklin et al., 2002), during which major alluviation episodes were correlated to cooling trends that lasted generally 10-15 ka and culminated with a massive discharge and deposition of debris. These cooling trends were followed by abrupt warming. During the first part of the warm and humid periods (climatic optimum), the strong runoff, due to the initial lack of vegetation, mobilized the available debris deposition. The resulting sediment overloading from the upstream point source resulted in a channel-bed aggradation (*i.e.* the *downfilling* of Schumm, 1993; Sugai, 1993). Afterward, a degradational stream behavior occur favored by: 1) late sediment-deficient basin discharge; 2) growth of the vegetation density improving infiltration capacity; 3) predominant canalized runoff. Streams entrench the older, proximal fan deposits transporting debris downfan to form secondary fans and producing flights of downward-stepping terrace surfaces (e.g. Sugai, 1993).

The drainage system that crosses the Düzce Fault runs from the Almacik Block mountain front to the Düzce basin through bajadas. Since the stream outlets are ~60 km from the coastline, the discharge regimes, or liberation of sediments, are likely not related to sea-level changes. Differently, relative tectonic lowering of the Düzce basin base-level (Efteni Lake-Golyaka area, Fig. 2; Pucci, 2007) may have contributed to the degradational behavior of the drainage system at the mountain front and to the formation of flights of downward-stepping terrace surfaces. During the

climatic optimums periods, the influence of climate on the upper reaches of the drainage network (*i.e.* hinterland sediment source of the Almacik Block) can compete with tectonics at the outlets to the Düzce basin. By providing a large discharge of sediments, climate overcomes the tectonic base-level lowering inducing aggradational rather than degradational behavior. Thus, drainage evolution and fan formation in the Düzce area is mainly climatically-controlled and related to the major alluviation episodes (optimums) in the Mediterranean region. Not far from our study area, in the central part of the Anatolian Plateau, several Authors (*e.g.* Roberts *et al.*, 1999; Kashima, 2002) recognized stream dynamics that can be compared with that of the Düzce area drainage system. In fact, they observed a degradational behavior following the early Holocene (7ka B.P.) alluvional phase, that produced flights of downward-stepping terrace surfaces inset and triggered woodland expansion over the open environment.

To date the geomorphic markers that are used to gauge the deformation through time we used both Radiocarbon and Optically Stimulated Luminescence (OSL) dating. Measurements were performed on samples collected in the upper layers composing the alluvial surfaces cut by deflected streams or river terraces. This implies that the true age of formation of terrace risers and stream entrenchments are subsequent to deposits they are incised in. On this light, the deposits we dated are systematically older than the offset geomorphic markers and the slip rate calculated by means of such ages should be considered a minimum.

4.1 The deflected drainage pattern

The Tilki-Cicubey (A) area is characterized by well-defined, 400 to 800 m long, elongated shutter ridges, along the base of the range front (e.g. spot x, Fig. 3). Most of these ridges, ~70 m high with steep slopes, are made of highly tectonized, Paleozoic-Jurassic granitoid unit.

The north-flowing drainage system of this area shows spectacular right-handed deflections of the streams that cross, with high angle, the elongated shutter ridges. These deflections are associated with the repeated motion of the shutter ridges, as they acted as natural dams to the streams flow. As a result, the streams are dragged along the fault line and their downstream reach move away from the flow axe of the related upstream reach. Tectonic influence on drainage pattern along the fault is also expressed by stream piracy. In fact, beheaded channels (*i.e.*, abandoned downstream reaches) flow through fault-parallel linear valleys and connect to the nearby stream, creating apparent sinistral deflections and perched ponding areas (spots s and p, respectively, in Fig. 3).

The analyzed morphologies portray piercing points that can be useful for slip rate calculation assuming an Holocene stream history as follows: 1) the stream was free to flow along a quasi-straight channel and to discharge alluvial deposits with aggradational behavior (Fig. 4a); 2) because of climatic influence the stream switches to degradational behavior and starts incising within the most recent alluvial surface, the channels remain entrenched and produce terrace remnants (Bull, 1991) (Fig. 4b); 3) being unable to change its course, the entrenched stream increase its deflection each time slip occurs on the fault it crosses (Ouchi, 2004 and 2005) (Fig. 4c).

To determine the accumulated strain, we measured the distance between the possible projection on the fault trace of the two stream channel axes that belongs to the two fault blocks (*e.g.* spot x, Fig. 3b). We measured the offsets directly in the field and using 2.5 m-resolution, panchromatic SPOT satellite imagery, geo-referenced by means of GIS (Geographic Information System).

Flow directions with high angles with respect to the strike of the Düzce Fault favors the preservation of the fault-related deflection (Allen, 1962). However, the measurement of the horizontal displacement is affected by uncertainties, such as: 1) an original watercourse not necessarily straight, as suggested by different crossing angles between the upstream and the downstream reaches and the fault; 2) erosion due to fluvial processes that can overcome the tectonic signal by straightening the stream course.

4.1.1. Measuring the offset

In the Tilki-Cicubey (A) area we investigated in detail two locations with similar features: the Amcahasanbey (1, Fig. 3) and the Cicubey sites (2, Fig. 3).

The Amcahasanbey site shows the alignment of the bedrock shutter ridge with a 10 meter high remnant of the Holocene alluvial deposits bounded to the south by a south-facing fault escarpment and showing an asymmetric profile as evidence of repeated deformation (Fig. 5). At this site, a stream flows north-eastward along an entrenched valley of the range front and when it crosses the fault, it turns east to flows along the fault zone. After about a hundred meters, it cuts the fault-controlled dam through an outlet to the Düzce Basin (1, Fig. 3 and 5).

Taking into consideration the assumptions and methods explained in the previous chapter, the measurement of the present-day Amcahasanbey channel deflection yields 105 ± 25 m (1, Fig. 3b). Also, the abandoned left wall of the channel, evidenced by an abrupt slope change between the bedrock ridge and the Holocene alluvial deposits remnant, can be correlated with an up stream channel wall (spot y and w, respectively, Figs. 4c and 5a) and yield a comparable offset of 104 ± 26 m.

The Cicubey site (2, Fig. 3) is an analogue of the previous site. The Düzce Fault offset a NNE-trending stream that is forced to turn sharply to the east under the control of the south-facing fault escarpment. The stream deeply incises a 15 m-high ridge, that acts as a shutter ridge (Fig. 6). This ridge is made of alluvial deposits that are the analogue of the Holocene alluvial remnant found at Amcahasanbey. Along the south-facing fault escarpment the stream shows an aggradational cut-and-fill behavior, with inset of young generation of terraces. The measured deflection of the present stream channel yields 105 ± 15 m (2, Fig. 3b; Fig. 6).

Area (A) comprises also two more right-hand stream deflections that yielded comparable cumulative offset measurements of 110 ± 22 m and 106 ± 34 m, that contribute to an overall average of about 106 ± 24 m (Fig. 3b).

4.1.2. Dating

In order to set the timing of the last depositional phase (prior to the stream entrenchment) that likely marks the onset of the stream deflection, the alluvial deposits of the Holocene alluvial remnants were dated. We dug two pits (0.6 and 0.8 m-deep, respectively) on top of the Amcahasanbey (1) and Cicubey (2) alluvial paleosurfaces (Figs. 4 and 6). The Amcahasanbey

site exposed 0.2-0.3 m of pristine hard carbonatic soil laying over a gray-brown organic silt with few rounded gravels. The Cicubey site showed 0.3-0.4 m of plowed silty soil laying over a brown organic silt. Samples were collected at the pit's bottom for radiocarbon dating. Since an insufficient amount of charcoal or charred organic material was available for dating using conventional decay-counting methods, the bulk organic matter was dated. About 100 g of sampled material from each site was sent to the Beta Analytic inc. laboratory for dating.

The samples were crushed, slurried and sieved prior to chemical pre-treatment and dating by decay counting (Table 1). The bulk sediment samples provided a radiocarbon age of 5870 ± 50 yr BP, for the Amcahasanbey paleosurface (1) and 4150 ± 35 yr BP for the Cicubey paleosurface (2). These ages have been calibrated by means of the radiocarbon program CALIB REV5.0.1 (Stuiver and Reimer, 1993), that provides 6720 ± 120 cal yr BP and 4670 ± 60 cal yr BP, respectively (2σ, Table 1). On the basis of geomorphic considerations these surfaces where expected to be coeval. The difference in radiocarbon age may derive from the intrinsic problems in dating bulk soil samples. In fact these represent composite ages (e.g. an average age for all of the organics in the sample) and, frequently, may have experienced post-depositional contamination with younger carbon that rejuvenates the true age (Matthews 1980; Polach *et al*. 1981; Rosholt *et al*. 1991).

Comparing these ages with the optimum in the climatic fluctuation during the Holocene (*i.e.*, favorable to channel aggradation) that presents a peak at ~7000 yr, the dating from Tilki-Cicubey area is taken as more

representative. Thus, if the 105 ± 25 m stream deflections developed during the past 6720 ± 120 cal yr BP, a slip rate of 15.7 ± 4 mm/yr is obtained.

4.2 The offset river terraces

At the Beykoy-Degirmenbası area, the Düzce Fault crosscuts a wide Pleistocene bajada that extends as far as 3 km north of the mountain-piedmont junction. There, the alluvial deposits reach an elevation of more than 130 m above the younger deposits of the Düzce Basin. Nowadays, this bajada is not depositionally active but is being eroded by the entrenched streams that flow through it and is overlapped by a young generation of alluvial fans. Here, the Düzce Fault forms a left step-over resulting in a 0.8 km-wide and 1.8 km-long pressure ridge (spot f, Fig. 7). This pressure ridge has an asymmetric cross profile, with a steep northern flank and a gentle southern flank. The northern flank was affected by the main 1999 coseismic ruptures, with a strike and dip slip offset components of about 4.0 m and 0.7 m, respectively (Akyuz et al., 2002; Duman et al., 2005; Pucci, 2007).

West of this Pleistocene bajada the Develi River outflows from the Almacik Block at around 210 m a.s.l. and, turning westward, flows toward the Efteni Lake (Fig. 2). The Develi River is one of the largest watercourse of the area. Its outlet to the Düzce Basin has been delivering sediments from the adjacent hinterland sediment source of the Almacik Block, where the uppermost reaches of the drainage network develop. Since this outlet is about 60 km from the coastline, the sea-level changes do not have a significant impact and the discharge regimes (*i.e.* liberation of sediments) are mostly upstream-controlled. Conversely, during the late Quaternary, the southwestern area of the Düzce Basin was the effective and direct local

base-level (Pucci, 2007). The tectonic subsidence of this local base-level, together with the dip-slip (north side down) component of the Düzce Fault (Pucci, 2007), contributed to the degradational behavior of the Develi River. In fact, the present-day morphology of the alluvial fan remnants at the Develi River outlet, shows the presence of a large Pleistocene fan, up to 2.5 km wide, whose sediments have been incised later by the formation of flights of downward-stepping terrace surfaces.

In contrast to the deflected drainage pattern of the Tilki-Cicubey area, the Develi River is sufficiently large to maintain its longitudinal profile by downcutting and keeping peace with the base-level changes and without preserving any fault-related stream deflection. Actually, large streams that show a degradational behavior have the ability to remove a large volume of sediments as well as any evidence for single coseismic displacement, during the interseismic period (*e.g.* Sugai, 1993). If this is the case, only features that are not more related to the present dynamic of the streams are suitable evidences for the ongoing deformation (*e.g.*, a flight of abandoned fluvial terraces; Van Dissen and Berryman, 1996).

At present, the Düzce Fault crosscut and shift the alluvial fan deposits far away from the path of the river, sheltering from erosion the northern terraces (Figs. 8a, b, c and d). The erosional scarps between two consecutive depositional surfaces (risers) can be observed at both sides of the Düzce fault (*e.g.* spot e, Fig. 7 and 9). By their correlation, these risers are geomorphic markers that offer suitable piercing points for cumulative offset determinations. To determine the accumulated strain, we measured the distances between the possible projections of the trajectories of the correlated terrace risers along the fault trace (*e.g.* spot x, Fig. 9a). We

measured the offsets using 2.5 m-resolution, panchromatic SPOT satellite imagery, geo-referenced by means of GIS (Geographic Information System). The relative elevation of the terraces was measured by means of a geodetic water level.

The measurement of the horizontal displacement is affected by some uncertainties, such as: 1) unknown original geometry of the terrace riser with respect to the fault trace; 2) modification the original geometry of the terrace riser by erosional processes; 3) terrace riser correlation.

4.2.1. Measuring the offset

North of the fault trace, we recognized three, clear-cut orders of terraces, whose morphology mimics the Develi River left turn, inset into a radial fan slope. The first order is the present-day floodplain (I, Fig. 7). The second order is a Holocene terrace, about 1.0 m higher than the present-day floodplain (II, Fig. 7). The third order is formed by a late Pleistocene flight of alluvial fan deposits, 7-10 m higher than the Holocene terrace (III, Fig. 7). The radial fan slope is the oldest and highest depositional surface, 10-15 m higher than the third terrace order, that decreases downfan with a convex-up profile (IV, Fig. 7). The young terrace surfaces are progressively inset and show a downward-stepping flights arrangement shaped by cut-and-fill alluvial behavior.

Three risers are found at the right side of the river outlet that degrade downfan (III-IV, II-III and I-II, respectively, Fig. 7). The displacement of the III-IV and II-III risers and the resultant morphological juxtaposition did not engaged any other important stream (i.e. capture) or strong erosional process, able to substantially modify them. Following this observation, we

correlated risers at both sides of the fault and we reconstructed their tectonic evolution (Fig. 7). For the III-IV and II-III order risers, we measured 890 ± 110 m and 300 ± 20 m offsets, respectively. The displacement of the I-II risers (175 ± 55 m) presents large uncertainties due to the ambiguous location of the northern escarpment, probably induced by anthropic or erosional modifications.

4.2.2. Dating

Since we expected probable ages close to or out of the limits of the radiocarbon dating method, we sampled the third and the fourth order of the terrace risers for Optically Stimulated Luminescence (OSL) dating method. To avoid possible reoccupation due to alluvial deposition over previously stable terrace surfaces and consequently rejuvenation of the surfaces, we sampled the highest terraces located south of the fault trace (Figs. 8 and 9b). Numerous studies (Jain et al., 2003 and reference therein) indicate the robustness of OSL method because it has yielded ages in agreement with other chronologic controls at least for the past ~100 ka. A luminescence age is a measure of the time elapsed since the exposure of the sediment to sunlight. The selection and sampling of sediment is a crucial step in the luminescence analysis. This alluvial fan contains clay-rich silt deposits amenable to dating. In fact, the alluvial system deposited a relatively thick and homogeneous unit that has not undergone significant diagenetic changes during burial. To insure luminescence integrity, we sampled sediment cores ~0.6 m below the surface, by hammering into the section, through a metal pipe, a black ABS pipe (5 cm diameter and 20 cm long), that we closed with end caps. In order to allow dose rate, mineralogic and granulometric analyses, we took additional 100 g samples from the same sampled layer

that have not be shielded from light exposure. The samples were dated at the Luminescence Laboratory, Department of Earth and Environmental Sciences, University of Illinois at Chicago (UIC).

The intensity of the luminescence was calibrated in the laboratory (Table 2) to yield an equivalent dose, which is divided by an estimate of the radioactivity that the sample received during burial (dose rate) to render a luminescence age. The Luminescence Laboratory of UIC evaluated the multiple aliquot additive dose method (MAAD) (e.g. Forman and Pierson, 2002) appropriate for equivalent dose determination of all samples, by means of infrared stimulation (880 ± 80 nm) on the fine-grained (4-11 micron) polymineral component. Resulting ages are 60,170 ± 6280 yr BP and 21,700 ± 1850 yr BP for the upper and the lower terraces, respectively (IV and III, Fig. 12) (1σ, Table 2). Even though constrained by a few dating samples, the ages used for slip rate calculations are consistent to the alluvional optimum in the climatic fluctuation. In fact, the correlated terrace flights of the study area result to be climatically-controlled, since the rivers alluviation phases occurred at the end of dry, cooling trends and the rivers degradational phases at the transition from arid to humid conditions (~60 ka, ~21 ka).

Summarizing, at the Beykoy-Degirmenbası area, the 300 ± 20 m and 890 ± 110 m measured offset coupled with their respective age 21,700 ± 1850 yr BP and 60,170 ± 6280 yr BP translate to slip rates of 14 ± 2.1 mm/yr and 15.2 ± 3.5 mm/yr, respectively.

5. Conclusions

Geomorphological mapping and dating of geomorphic markers along the eastern section of the Düzce Fault provide the first, although preliminary, information on the slip rate of this part of the NAFZ.

We mapped four streams deflected ~100 m by the Düzce fault and radiocarbon dated the alluvial deposits of the paleosurface that represents the onset of the deflection at 6720 ± 120 yr BP. This age and the amount of stream deflection yield a slip rate of 15.7 ± 4 mm/yr.

In addition, we documented the Düzce Fault crosscutting the terrace risers incised by the Develi River throughout Late Pleistocene alluvial deposition. The offset of the two oldest correlated terrace risers is ~300 and 890 m, respectively. By means of OSL, we dated the alluvial deposits of the terraces, which represent the onset of right-lateral tectonic shift, at 21,700 ± 1850 yr BP and 60,170 ± 6280 yr BP. These ages and offsets translate to slip rates of 14 ± 2.1 mm/yr and 15.2 ± 3.5 mm/yr, respectively.

Even though dating is limited and related assumptions rather simplistic, the fact these ages are consistent to the alluvional optimums in the climatic fluctuation (~60 ka, ~21 ka, 7 ka BP) in the Mediterranean area increases substantially their level of confidence.

Although the calculated slip rates span ages of 7000 up to 60 ka BP, these values are similar. Assuming a constant slip rate for the past 60 ka, the mathematical linear regressions that interpolate the maximum and the minimum slip rate intervals yield values of 18.2 and 11.8 mm/yr, respectively. These results translate into a mean slip rate of 15.0 mm/yr ± 3.2 mm/yr (Fig. 10).

Interestingly, this slip rate, derived at sites where the 1999 offset was of ~4 m, compares well with the 11.8-15.2 mm/yr paleoseismological slip

rate derived for the past 2000 yr from the average recurrence time (320-390 yr) and maximum 1999 coseismic slip (~5 m) (Pantosti et al., 2007).

Assuming that the GPS measured strain accumulation (at short time-scales) due to the plate motion along this part of the NAFZ is relatively uniform and constant over the last 60 ka, and is completely released by the Mudurnu (to the south) and the Düzce (to the north) parallel faults (Fig. 1), the Düzce Fault accommodates more than half of the total GPS slip-rate estimates. This indicates that the Düzce Fault importantly participates to the North Anatolian margin deformation, implying slip partitioning between Mudurnu and Düzce faults through a duplex structural style (Woodcock and Fischer, 1986). These results open new questions about: (i) the temporal fault interactions between the Mudurnu and the Düzce faults, as an interlinked seismogenic system; (ii) the relative role of these faults in the seismic hazard of the area; (iii) the cause of the structural style along this part of the NAFZ and its inception in the plate boundary evolution.

Acknowledgements

This research is supported by the European Commission Project “Relief”: Large earthquake faulting and implications for seismic hazard assessment in Europe: The Izmit-Düzce earthquake sequence of 1999, Turkey, Mw 7.4, 7.1, EVG1-CT-2002-00069. We thanks to the anonymous reviewers for their acute suggestions that strongly augmented the quality of this manuscript.

References

Akyüz, H.S., A.A. Barka, E. Altunel, R.D. Hartleb, and G. Sunal, 2000. Field observations and slip distribution of the November 12, 1999 Düzce earthquake (M=7.1), Bolu - Turkey. In: A.A. Barka et al. (Eds.), The 1999 Izmit and Düzce earthquakes; preliminary results. Istanbul Technical University, Istanbul, Turkey, pp. 63-70.

Akyüz, H.S., R.D. Hartleb, A.A. Barka, E. Altunel, G. Sunal, B. Meyer and R. Armijo, 2002. Surface rupture and slip distribution of the 12 November 1999 Düzce earthquake (M7.1), North Anatolian Fault, Bolu, Turkey. Bull. Seism. Soc. Am. 92 (1), 61-66.

Aitken, M.J. and S.G.E. Bowman, 1975. Thermoluminescent dating: Assessment of alpha particle contribution. Archaeometry 17, 132-138.

Allen, C.R., 1962. Circum-Pacific faulting in the Philippines–Taiwan region. J. Geophy. Res. 67, 4795–4812.

Ambraseys, N.N., 1970. Some characteristic features of the North Anatolian fault zone. Tectonophysics 9, 143-165.

Ambraseys N.N, 2002. The seismic activity of the Marmara Sea region over the last 2000 years. Bull. Seism. Soc. Am. 92 (1), 1-18.

Ambraseys N.N. and C.F. Finkel, 1995. The seismicity of Turkey and adjacent areas: a historical review, 1500-1800. Muhittin Salih Eren, Istanbul, pp. 240.

Armijo R., B. Meyer, A. Hubert and A.A. Barka, 1999. Westward propagation of the North Anatolian fault into the northern Aegean: Timing and kinematics. Geology 27 (3), 267-270.

Ayhan, M.A., C. Demir, A. Kilicoglu, I. Sanli, and S.M. Nakiboglu, 1999. Crustal motion around the western segment of the north Anatolian fault zone: geodetic measurements and geophysical interpretation. International Union of Geodesy and Geo-physics (IUGG99), Birmingham, United Kingdom, 18-30 July.

Ayhan, M.E., R.B¨urgmann, S. McClusky, O. Lenk, B. Aktug, E. Herece and R.E. Reilinger, 2001. Kinematics of the Mw = 7.2, 12 November 1999, Düzce, Turkey earthquake. Geophys. Res. Lett. 28 (2), 367-370.

Barka, A.A., 1992. The North Anatolian fault zone. Annales Tectonicae 6, 164-195.

Barka, A.A. and L. Gulen, 1989. Complex evolution of the Erzincan Basin (eastern Turkey). J. Struct. Geol. 11 (3), 275-283.

Blum, M.D. and T.E. Törnqvist, 2000. Fluvial responses to climate and sea-level change: a review and look forward. Sedimentology 47, 2-48.

Bull, W.B., 1991. Geomorphic responses to climatic change. London, Oxford University Press, pp. 326.

Burbank, D.W., and R.S. Anderson, 2001. Tectonic geomorphology. Blackwell Science, Inc. pp.274.

Canitez, N. and B. Ucer, 1967. Computer determinations for the fault plane solutions in and near Anatolia. Tectonophysics 4, 235-244.

Dewey, J.F., M.R. Hempton, W.S.F. Kidd, F. Saroglu and A.M.C. Şengör, 1986. Shortening of continental lithosphere; the neotectonics of eastern Anatolia, a young collision zone. Geological Society Spec. Pub. 19, 3-36.

Dhont, D., J. Chorowicz, T. Yürür, O. Köse, 1998. Polyphased block tectonics along the North Anatolian Fault in the Tosya basin area (Turkey). Tectonophysics 299, 213–227.

Duman, T., Ö. Emre, A. Dogan and S., 2005. Step-over and bend structures along the 1999 Düzce earthquake surface rupture, North Anatolian Fault, Turkey. Bull. Seism. Soc. Am. 95 (4), 1250-1262.

Erin¸c, S., 1953. Doğu Anadolu Coğrafyası: Istanbul Univ. Yayın No. 572, Istanbul Univ. Edeb. Fak. Coğraf. Enst. Yayin, 15, Istanbul, pp. 124. (in Turkish)

Forman, S.L., and J. Pierson, 2002. Late Pleistocene luminescence chronology of loess deposition in the Missouri and Mississippi river valleys, United States. Palaeogeography Palaeoclimatology Palaeoecology 186 (1-2), 25-46.

Gaudemer, Y., P. Tapponnier and D.L. Turcotte, 1989. River offsets across active strike-slip faults. Annales Tectonicae 3 (2), 55-76.

Herece, E., and E. Akay, 2003. 1:100.000 geological maps of the North Anatolian Fault. General Directorate of Mineral Research and Exploration, Ankara, Appendix 3 and 4.

Huang, W., 1993. Morphologic patterns of stream channels on the active Yishi Fault, southern Shandong Province, eastern China: implication for repeated great earthquakes in the Holocene. Tectonophysics 219, 283– 304.

Hubert-Ferrari, A., R. Armijo, G. King, B. Meyer and A. Barka, 2002. Morphology, displacement, and slip rates along the northern Anatolian Fault, Turkey. J. Geophys. Res. 107 (B10), 2235, doi: 10.1029/2001JB000393.

Jackson, J. and D. McKenzie, 1988. The relationship between plate motions and seismic moment tensors, and the rates of active deformation in the Mediterranean and Middle East. Geoph. J. Int. 93 (1), 45-73.

Jackson, J., R. Norris, J. Youngson, 1996. The structural evolution of active fault and fold systems in central Otago, New Zealand: evidence revealed by drainage patterns. J. Struct. Geol. 18, 217– 234.

Jain, M., L. Botter-Jensen and A.K. Singhvi, 2003. Dose evaluation using multiple-aliquot quartz OSL: test of methods and a new protocol for improved accuracy and precision. Radiation Measurements 37, 67-80.

Johnson, A. M., R. W. Fleming, and K. M. Cruikshank, 1994. Shear zones formed along long, straight traces of fault zones during the 28 June 1992 Landers, California, earthquake. Bull. Seism. Soc. Am. 84**,** 499–510.

Kahle H. G., M. Cocard, Y. Peter, A. Geiger, R. Reilinger, S.C. McClusky, R. King, A. Barka and G. Veis, 1999. GPS-derived strain rate field within the boundary zones of the Eurasian, African, and Arabian Plates. J. Geophy. Res. 105 (B3), 23 353-23 370.

Kahle H. G., M. Cocard, Y. Peter, A. Geiger, R. Reilinger, A. Barka and G. Veis, 2000. GPS-derived strain rate field within the boundary zones of the Eurasian, African, and Arabian Plates. J. Geophy. Res. 105 (B3), 23 353-23 370.

Kashima, K., (2002), Environmental and climatic changes during the last 20,000 years at Lake Tuz, central Turkey, Catena, 48, 3–30.

Keller, E.A., M.S. Bonkowski, R.J. Korsch and R.J. Shlemon, 1982. Tectonic geomorphology of the San Andreas fault zone in the southern Indio Hills, Coachella Valley, California. Geol. Soc. Am. Bull. 93, 46-56.

Komut T., 2005. Paleoseismological studies on Düzce fault and geological data on the seismogenic sources in the vicinity of Düzce area. Kandilli Observatory and Earthquake Research Institute Boğaziçi University, Ph.D. Thesis, pp. 155.

Ikeda, Y, Y. Suzuki, E. Herece, F. Saroglu, A.M. Isikara and Y. Honkura, 1991. Geological evidence for the last two faulting events on the North Anatolian fault zone in the Mudurnu Valley, western Turkey. Tectonophysics 193 (4), 335-345.

IrrlitzW., 1972. Lithostratigraphie und tektonische Entwicklung des Neogens in Nordostanatolien (Känozoikum und Braunkohlen in der Türkei. 6.). Beih. Geol. Jahrb. 120, 111 pp.+10 plates. (in German)

Lazarte, C.A., J.D. Bray, A.M. Johnson, and R.E. Lemmer, 1994. Surface breakage of the 1992 Landers earthquake and its effects on structures. Bull. Seism. Soc. Am 84**,** 547–561.

Le Pichon, X., A.M.C. Şengör, E. Demirbag, C. Rangin, C. İmren, R. Armijo, N. Görür, N. Çağatay, B. Mercier de Lepinay, B. Meyer, R. Saatçılar and B. Tok, 2001. The active Main Marmara Fault. Earth and Planetary Science Letters 192, 595-616.

Macklin, M.G., I.C. Fuller, J. Lewin, G.S. Maas, D.G. Passmore, J. Rose, J.C. Woodward, S. Black, R.H.B. Hamlin, J.S. Rowan, 2002. Correlation of fluvial sequences in the Mediterranean basin over the last 200 ka and their relationship to climate change. Quaternary Science Reviews, 21, 1633–1641.

Matsuda T., 1967. Cumulative displacement of river gorges by active fault. Journal of the Geological Society of Japan 73 (2), pp.121.

Matthews, J. A, 1980. Some problems and implication of 14C dates from a podzol buried beneath an end moraine at Haugabreen, southern Norway. Geografiska Annaler 62°, 185-208.

McClusky, S.C., A. Balassanian, A.A. Barka, C. Demir and S. Ergintav, 2000. Global positioning system constrain on plate kinematics and dynamics in the eastern Medditerranean and Caucasus. J. Geophy. Res. 105 (B3), 5695-5720.

McKenzie, D.P., 1972. Active tectonics of the Mediterranean region. Geophys. J. R. Astron. Soc. 30, 109-185.

Okay, A.l., E. Demirbag, H. Kurt, N. Okay, I. Kuscu, 1999. An active, deep marine strike-slip basin along the North Anatolian Fault in Turkey. Tectonics 18 (1), 129-147

Ouchi, S., 2004. Flume experiments on the horizontal stream offset by a strike-slip fault. Earth Surface Processes and Landforms 29, 161– 173.

Ouchi, S., 2005. Development of offset channels across the San Andreas fault. Geomorphology 70, 112– 128.

Pantosti, D., S. Pucci, N. Palyvos, P.M. De Martini, G. D'Addezio, P.E.F. Collins, C. Zabci, 2007. Paleoearthquakes of the Düzce fault (North Anatolian Fault Zone): implications for earthquake recurrence. J. Geophys. Res., in press.

Polach, H., J. Golson, and J. Head, 1981. Radiocarbon Dating: A Guide for Archaeologists on the Collection and Submission of Samples and Age-Reporting Practices, in Australian Field Archaeology: A Guide to Techniques. Australian Institute of Aboriginal Studies. Canberra, Australia, 145-152.

Polonia A., L. Gasperini, A. Amorosi, E. Bonatti, G. Bortoluzzi, N. Çagatay, L. Capotondi, M.-H. Cormier, N. Görür, C. McHugh, L. Seeber, 2004. Holocene slip rate of the North Anatolian Fault beneath the Sea of Marmara. Earth and Planetary Science Letters 227, 411– 426.

Pucci S., 2007. The Düzce segment of the North Anatolian Fault Zone (Turkey): understanding its seismogenic behavior through earthquake geology, tectonic geomorphology and paleoseismology. Ph.D Thesis, University of Perugia, Italy.

Pucci, S., Palyvos, N., Zabci, C., Pantosti, D., and M. Barchi, 2006. Coseismic ruptures and tectonic landforms along the Düzce segment of the North Anatolian Fault Zone (Ms 7.1, Nov. 1999). J. Geophys. Res., 111, B06312, doi:10.1029/2004JB003578.

Reilinger, R.E., S.C. McClusky, M.B. Oral, W. King and M.N. Toksöz, 1997. Global Positioning, System measurements of present-day crustal movements in the Arabian-Africa-Eurasia plate collision zone. J. Geophy. Res. 102 (B5), 9983-9999.

Reilinger, R.E., Toksöz, M.N., McClusky and A.A. Barka, 2000. 1999 Izmit, Turkey Earthquake was no surprise. GSA Today 10, 1-6.

Reimer, P.J., M.G.L. Baillie, E. Bard, A. Bayliss, J.W. Beck, C. Bertrand, P.G. Blackwell, C.E. Buck, G. Burr, K.B. Cutler, P.E. Damon, R.L. Edwards, R.G. Fairbanks, M. Friedrich, T.P. Guilderson, K.A. Hughen, B. Kromer, F.G. McCormac, S. Manning, C. Bronk Ramsey, R.W. Reimer, S. Remmele, J.R. Southon, M. Stuiver, S. Talamo, F.W. Taylor, J van der Plicht and C.E. Weyhenmeyer, 2004. IntCal04 terrestrial radiocarbon age calibration, 0-26 cal kyr BP. Radiocarbon 46, 1029-1058.

Reinecker, J., O. Heidbach, M. Tingay, P. Connolly, and B. Müller, 2004. The 2004 release of the World Stress Map (available online at www.world-stress-map.org)

Ritter, J.B., J.R. Miller and J. Husek-Wulforst, 2000. Environmental controls on the evolution of alluvial fans in Buena Vusta Valley, North Central Nevada, during late Quaternary time. Geomorphology 36, 63-87.

Roberts, N., S. Black, P. Boyer, W.J. Eastwood, H.I. Griffiths, H.F. Lamb, M.J. Leng, R. Parish, J.M. Reed, D. Twigg, and H. Yiğitbaşioğlu, 1999. Chronology and stratigraphy of Late Quaternary sediments in the Konya Basin, Turkey: Results from the KOPAL Project. Quaternary Science Reviews 18, 611-630.

Rosholt, J.N., S.M. Colman, M. Stuiver, P.E. Damon, C.W. Naeser, N.D. Naeser, B.J. Szabo, D.J. Muhs, J.C. Liddicoat, S.L. Forman, M.N. Machette, and K.L. Pierce, 1991. Dating methods applicable to the Quaternary. In: Morrison, R.B., (Ed.), Dating Methods Applicable to the Quaternary. The Geology of North America, vol. K-2, 45-74, Geological Society of America, Boulder, Colorado.

Şaroğlu, F., Ö. Emre and İ. Kuşçu, 1992. Active fault map of Turkey. General Directorate of Mineral Research and Exploration, Ankara.

Schumm, S.A., 1993. River response to baselevel change; implications for sequence stratigraphy. Journal of Geology 101 (2), 279-294.

Şengör, A.M.C., 1979. The North Anatolian transform fault: Its age, offset and tectonic significance. J. Geol. Soc. London 136, 269-282.

Şengör, A.M.C., N. Görür and F. Şaroğlu, 1985. Strike-slip faulting and related basin formation in zones of tectonic escape; Turkey as a case study. In Biddle, K.T., and N. Christie-Blick (Eds.) Strike-slip Deformation, Basin Formation and Sedimentation. Soc. Econ. Paleont. Min. Spec. Publ. 37, 227-264.

Şengör, A.M.C., O. Tüysüz, C. İmren, M. Sakınç, H. Eyidoğan, N. Görür, X. Le Pichon and C. Rangin, 2005. The North Anatolian Fault: a new look. Annu. Rev. Earth Planet. Sci. 33, 37-112.

Seymen, I., 1975. Tectonic characteristics of the North Anatolian fault zone in the Kelkit valley, Ph.D. thesis, Istanbul Technical Univ., Istanbul, Turkey, pp. 192.

Sieh, K.E., R.H. Jahns, 1984. Holocene activity of the San Andreas fault at Wallace Creek, California. Geol. Soc. Am. Bull. 95, 883– 896.

Sieh, K.L., L. Jones, E. Hauksson, K. Hudnut, D. Eberhart-Phillips, T.H. Heaton, S. Hough, K. Hutton, H. Kanamori, A. Lilje, S. Lindvall, S.F. McGill, J. Mori, C. Rubin, J.A. Spotila, J. Stock, H.K. Thio, J. Treiman, B. Wernicke, and J. Zachariasen, 1993. Near-field investigations of the Landers earthquake sequence, April to July, 1992. Science 260**,** 171–176.

Straub, C., H. G. Kahle, and C. Schindler, 1997. GPS and geologic estimates of the tectonic activity in the Marmara Sea region, NW Anatolia. J. Geophys. Res. 102 (B12), 27 587-27 601.

Stuiver, M., and P.J. Reimer, 1993. Extended (super 14) C data base and revised CALIB 3.0 (super 14) C age calibration program. Radiocarbon 35, 215-230.

Sugai, T., 1993, River terrace development by concurrent fluvial processes and climate change. Geomorphology, 6, 243-252.

Tatar Y., 1978. Kuzey Anadolu Fay Zonunun Erzincan-Refahiye arasindaki bölümü üzerinde tektonik incelemeler. Yerbilimleri 4, 201–36.(in Turkish)

Tchalenko, J.S., and N.N. Ambraseys, 1970. Structural analysis of the Dasht-e Bayaz, Iran, earthquake fractures. Geol. Soc. Am. Bull. 81, 41–60.

Tchalenko, J.S., and M. Berberian, 1975. Dasht-e Bayaz fault, Iran: earthquake and earler related structures in bedrock. Geol. Soc. Am. Bull. 86, 703–709.

Van Dissen, R., and K.R. Berryman, 1996. Surface rupture earthquakes over the last ~1000 years in the Wellington region, New Zealand, and implications for ground shaking hazard. J. Geophys. Res., 101, B3, 5999-6019.

Wallace, R.E., 1968. Notes on stream channels offset by the San Andreas fault, southern Coast Ranges, California. In: Dickinson, W.R., and A.

Grantz (Eds.), Conference on Geologic Problems of the San Andreas Fault System. Stanford University Publication in Geological Sciences 11, 6– 21.

Westaway, R., 1994. Present-day kinematics of the Middle-East and Eastern Mediterranean. J. Geophys. Res. 99, 12 071-12 090.

Wong, H K, T. Luedmann, A. Ulug and N. Gorur, 1995. The Sea of Marmara; a plate boundary sea in an escape tectonic regime. Tectonophysics 244 (4), 231-250.

Woodcock, N.H., and M. Fischer, 1986. Strike-slip duplexes. J. Struct. Geol. 8 (7), 725-735.

Yoshioka, T., K. Okumura and I. Kuscu, 1991. Trench excavation of the North Anatolian Fault, Turkey. Chishitsu News 4 (440), 60-66.

Captions

Figure 1

a) Tectonic setting of the eastern Mediterranean and continental extrusion of the Anatolian plate. Current motion relative to Eurasia (GPS (Global Positioning System) and SLR (Satellite Laser Ranging) velocity vectors, in mm/yr, from Reilinger et al., 1997)(modified from Armijo et al., 1999). b) Slip rate distribution along the North Anatolian Fault Zone (NAFZ). Different symbols are used on the basis of the time-scale and type of measured offset. Thin bars indicate uncertainties of the measurements. Numbers refer to slip rates from: (1) Armijo et al. (1999); (2) Polonia et al. (2004); (3) and (5) (Hubert-Ferrari et al., 2002); (4) Dhont et al. (1998); (6) to (9), (12) and (13) Erinc (1953), Gaudemer et al. (1989), Barka and Gulen, (1989), Huber-Ferrari et al. (2002) and Şengör et al. (2005); (10) and (11) Irrlitz (1972), Seymen (1975), Tatar (1978), Barka, (1992), Westaway (1994) and Hubert-Ferrari et al. (2002).

Figure 2

1999 fault scarp trace of the two parts of the Düzce Fault that can be divided in a western and eastern sections (dashed rectangles) (see Pucci, 2007). The eastern section shows localized slip whereas the western section slip is more diffused. Late Pliocene-Holocene continental deposits (compilation by 1:20 000 scale field survey and by Herece and Akay (2003)) and main drainage features of the Düzce basin are reported. Epicenter location (stars) and focal mechanism solutions from Harvard CMT. Shaded relief based on digital elevation model (DEM, interpolated from 10 m contours and auxiliary 5 m

contours of 1:25 000 scale topographic maps). Contour interval 100 m. (see Fig. 1b for location).

Figure 3

a) Simplified geomorphological map of the Tilki-Cicubey area. Contour interval 10 m. Letters indicate locations discussed in the text. (see Fig. 2 for location). b) Stream (white solid line) deflection measurements. Dashed lines indicate the possible projections on the fault (black solid line) of the stream channels. Dotted lines indicate the piercing points used for offset calculations. 1:18.000 scale aerial-photo on the background.

Figure 4

Schematic reconstruction of the recent stream history at the Amcahasanbey site (1 in Fig. 3). a) Late Pleistocene-Early Holocene: the stream flows and deposits along a quasi-straight channel; b) Holocene (~7000 yr): the stream starts to incise; c) Present: the stream is entrenched and right-hand deflected by the fault. (see Fig. 3 for location).

Figure 5

Views of the Amcahasanbey site (1 in Fig. 3). a) aerial view of the deflected stream. The channel walls used as piercing points (y and w) to measure the stream offset are reported. Dashed lines indicate the possible projections on the fault (black arrows) of the stream walls. b) view of the shutter ridge and of the dammed area. Small black arrows point to the coseismic rupture trace. Hexagon indicates the radiocarbon sample location. (see Fig. 3 for view directions).

Figure 6

Aerial view of the deflected stream at the Cicubey site (2 in Fig. 3). Small black arrows point to the coseismic rupture trace. Dashed lines indicate the possible projections on the fault (black arrows) of the stream channels. Hexagon indicates the radiocarbon sample location. (see Fig. 3 for view direction).

Figure 7

Simplified geomorphological map of the Beykoy-Degirmenbası area. Contour interval 10 m. (see Fig. 2 for location).

Figure 8

Schematic chronological reconstruction of the geometry of the Beykoy-Degirmenbası area (see Fig. 2 for location). The Düzce Fault has been crosscutting and right-laterally shifting the terrace flights and risers of the north-eastern side, that were sheltered from erosion. a) Late Pleistocene: the Develi River deposit a large alluvial fan, building a bajada at the base of the range front; b) Late Pleistocene (60 to 20 ka): the Develi River starts to incise the fourth order terrace deposits (IV) and to construct the younger, lower third order terrace (III) until 20 ka; c) Late Pleistocene (20 ka) to Holocene: the Develi River starts to incise the Late Pleistocene (20 ka) third order terrace (III) and to construct the Holocene terrace (II). d) Late Holocene: the Develi River incises the Holocene deposits of the second order (II) and to construct the present terrace (I). Risers IV-III and III-II are all severely offset.

Figure 9

a) Terrace risers offset at the Beykoy-Degirmenbası area. Dashed lines indicate the possible projections on the fault of the terrace risers. Dotted lines indicate the piercing points used for offset calculations. 1:18.000 scale aerial-photo on the background. b) Oblique view of the pressure ridge and the terrace risers (see Fig. 9a for view direction). Labels III and IV refer to terrace order. Small black arrows point to the coseismic rupture trace. Gray hexagons locates sampling sites.

Figure 10

Slip rate diagram of the Düzce Fault. The slip rates calculated at different time-scales are reported along with the interpolated uniform slip rate.

Table 1.

Radiocarbon ages and associated chronologic data for sediments from the Tilki-Cicubey area. The calibrated ages are calculated for the probability density function at the 95.4 per cent confidence limit (2σ).

Table 2.

Optically stimulated luminescence (OSL) ages and associated chronologic data for sediments from the Beykoy-Degirmenbası area. [a)] Blue emissions are measured with 3-mm-thick Schott BG-39 and one, 3-mm-thick Corning 7-59 glass filters that blocks >90% luminescence emitted below 390 nm and above 490 nm in front of the photomultiplier tube. [b)] The stability of the laboratory beta-induced (Gy) luminescence signal after preheating and

storage was tested by comparing luminescence emissions of immediately after preheating (10 hours at 150 ºC) and with at least a 30 day storage. A thermal stability ratio 1.06 -0.94 indicates little or no signal instability, within analytical resolution. [c)] Measured alpha efficiency factor as defined by Aitken and Bowman (1975). [d)] U and Th values calculated from alpha count rate, assuming secular equilibrium. K20 % determined by ICP-MS, Activation Laboratory Ltd., Ontario. [e)] Contains a cosmic rate dose rate component of 0.20 ± 0.02. [f)] All errors are at one sigma.

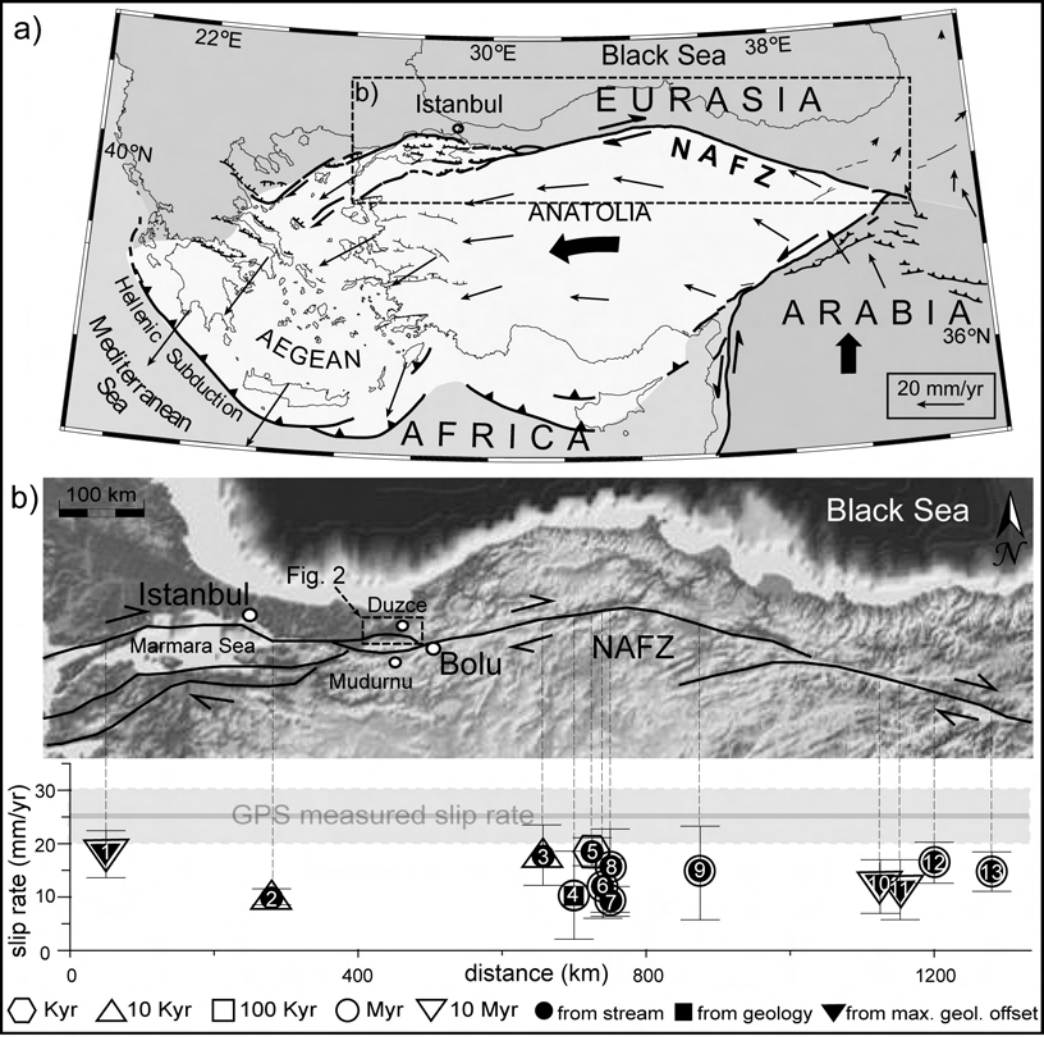
a)
22°E
30°E
Black Sea
38°E
b)
Istanbul
EURASIA
40°N
NAFZ
ANATOLIA
Hellenic Subduction
Mediterranean Sea
AEGEAN
ARABIA
36°N
20 mm/yr
AFRICA
b)
100 km
Black Sea
N
Istanbul
Fig. 2
Duzce
Marmara Sea
Bolu
NAFZ
Mudurnu
GPS measured slip rate
slip rate (mm/yr)
30
20
10
0
0
400
distance (km)
800
1200
1
2
3
4
5
6
7
8
9
10
11
12
13
Kyr
10 Kyr
100 Kyr
Myr
10 Myr
from stream
from geology
from max. geol. offset

Fig. 1

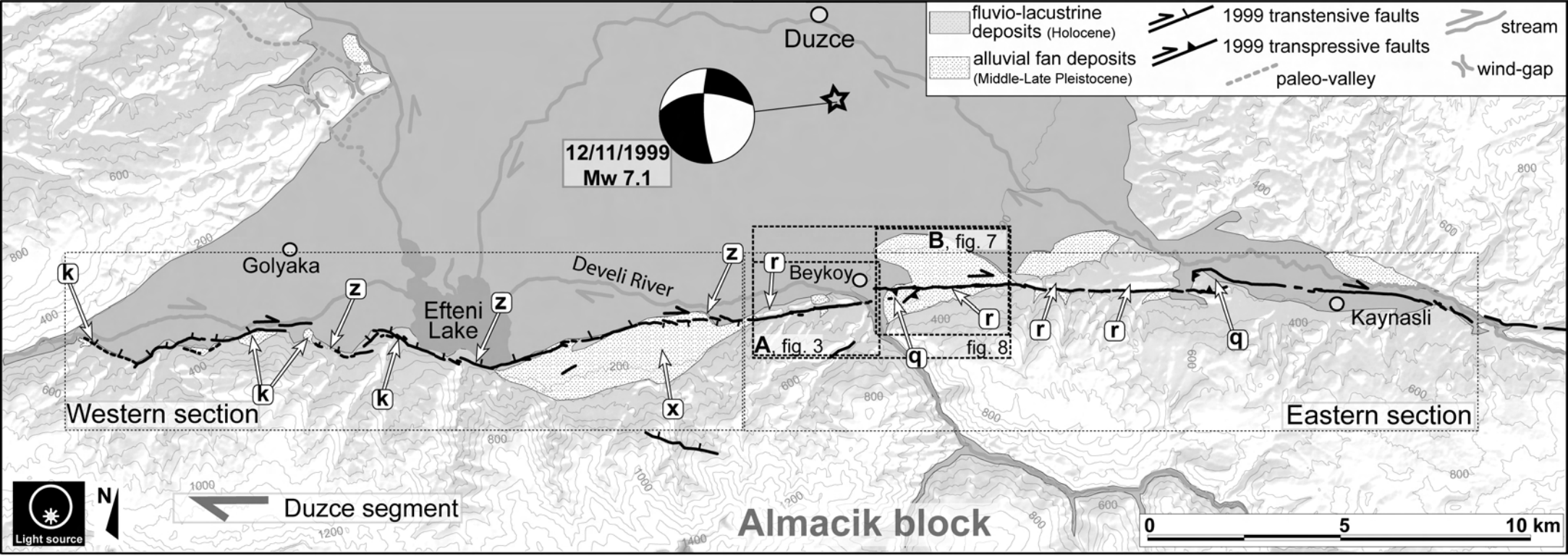
fluvio-lacustrine deposits (Holocene)
alluvial fan deposits (Middle-Late Pleistocene)
1999 transtensive faults
1999 transpressive faults
paleo-valley
stream
wind-gap
Duzce
12/11/1999
Mw 7.1
Golyaka
Develi River
Efteni Lake
Beykoy
Kaynasli
B, fig. 7
A, fig. 3
fig. 8
Western section
Eastern section
Duzce segment
Almacik block
Light source
N
0
5
10 km

Fig. 2

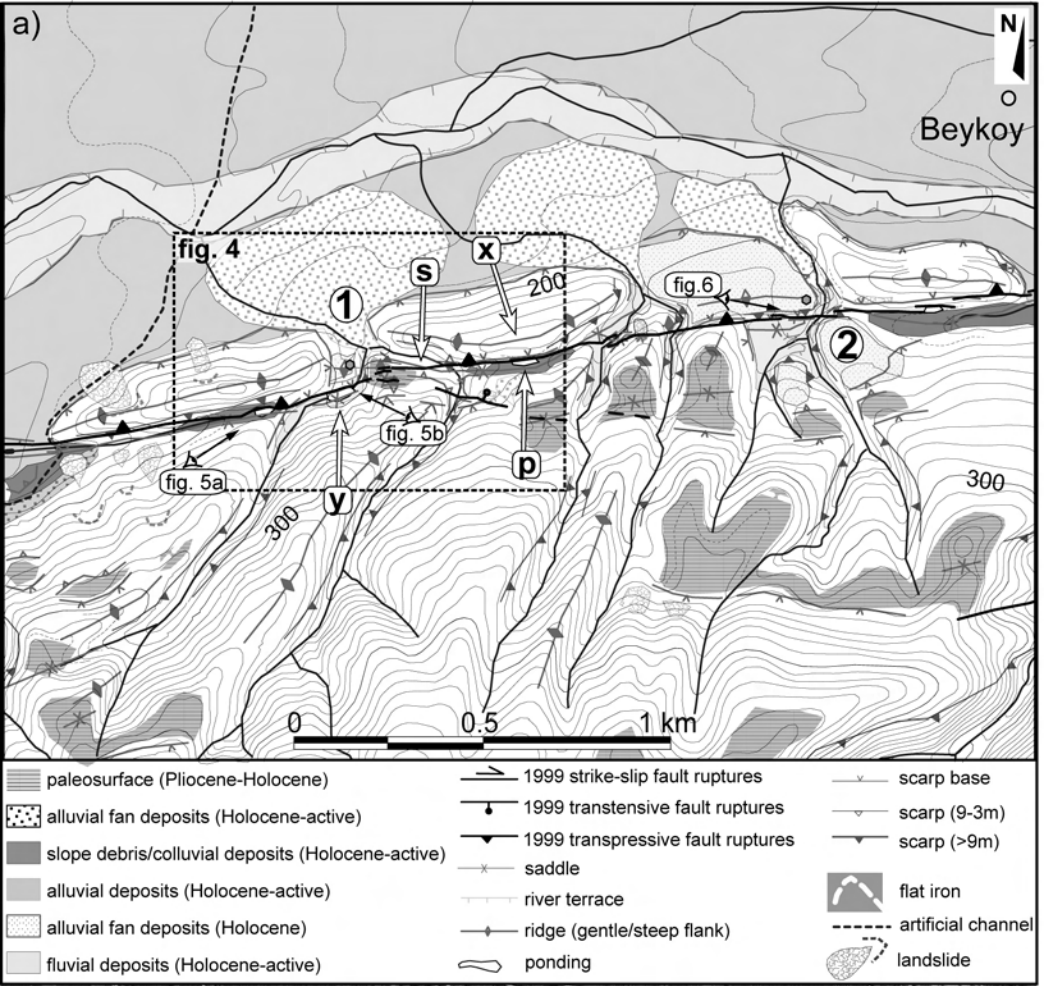
a)
N
Beykoy
fig. 4
x
s
1
200
fig.6
2
fig. 5b
fig. 5a
p
y
300
300
0
0.5
1 km
paleosurface (Pliocene-Holocene)
alluvial fan deposits (Holocene-active)
slope debris/colluvial deposits (Holocene-active)
alluvial deposits (Holocene-active)
alluvial fan deposits (Holocene)
fluvial deposits (Holocene-active)
1999 strike-slip fault ruptures
1999 transtensive fault ruptures
1999 transpressive fault ruptures
saddle
river terrace
ridge (gentle/steep flank)
ponding
scarp base
scarp (9-3m)
scarp (>9m)
flat iron
artificial channel
landslide

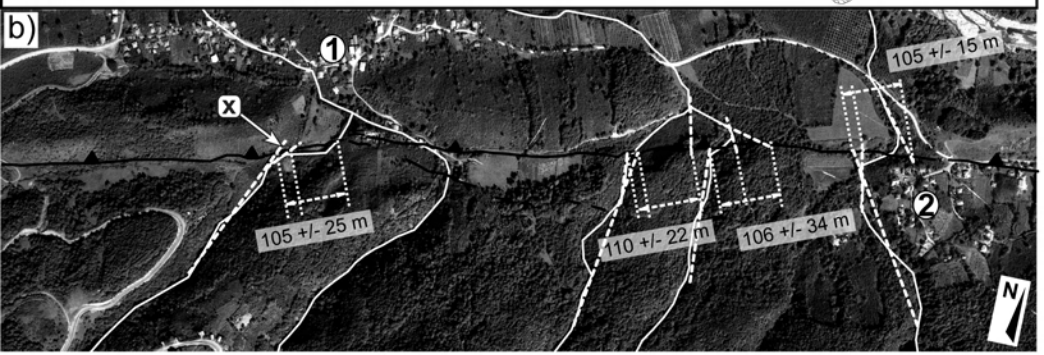
b)
1
x
105 +/- 25 m
110 +/- 22 m
106 +/- 34 m
105 +/- 15 m
2
N

Fig. 3

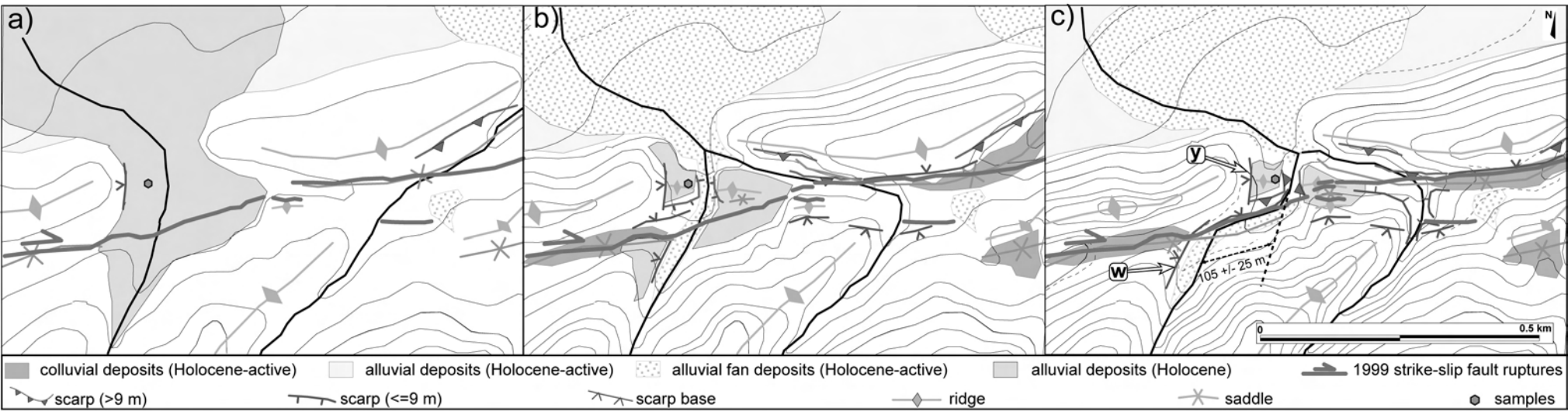
a)
b)
c)
N
y
w
105 +/- 25 m
0
0.5 km
colluvial deposits (Holocene-active)
alluvial deposits (Holocene-active)
alluvial fan deposits (Holocene-active)
alluvial deposits (Holocene)
1999 strike-slip fault ruptures
scarp (>9 m)
scarp (<=9 m)
scarp base
ridge
saddle
samples

Fig. 4


a)
Holocene alluvial surface
fig. 5b
N
y
105 +/- 25 m
104 +/- 26 m
1
bedrock shutter ridge
Holocene alluvial surface
w
b)
bedrock shutter ridge
Holocene alluvial surface
N
stream entrenchment
coseismic ponding

Fig. 5

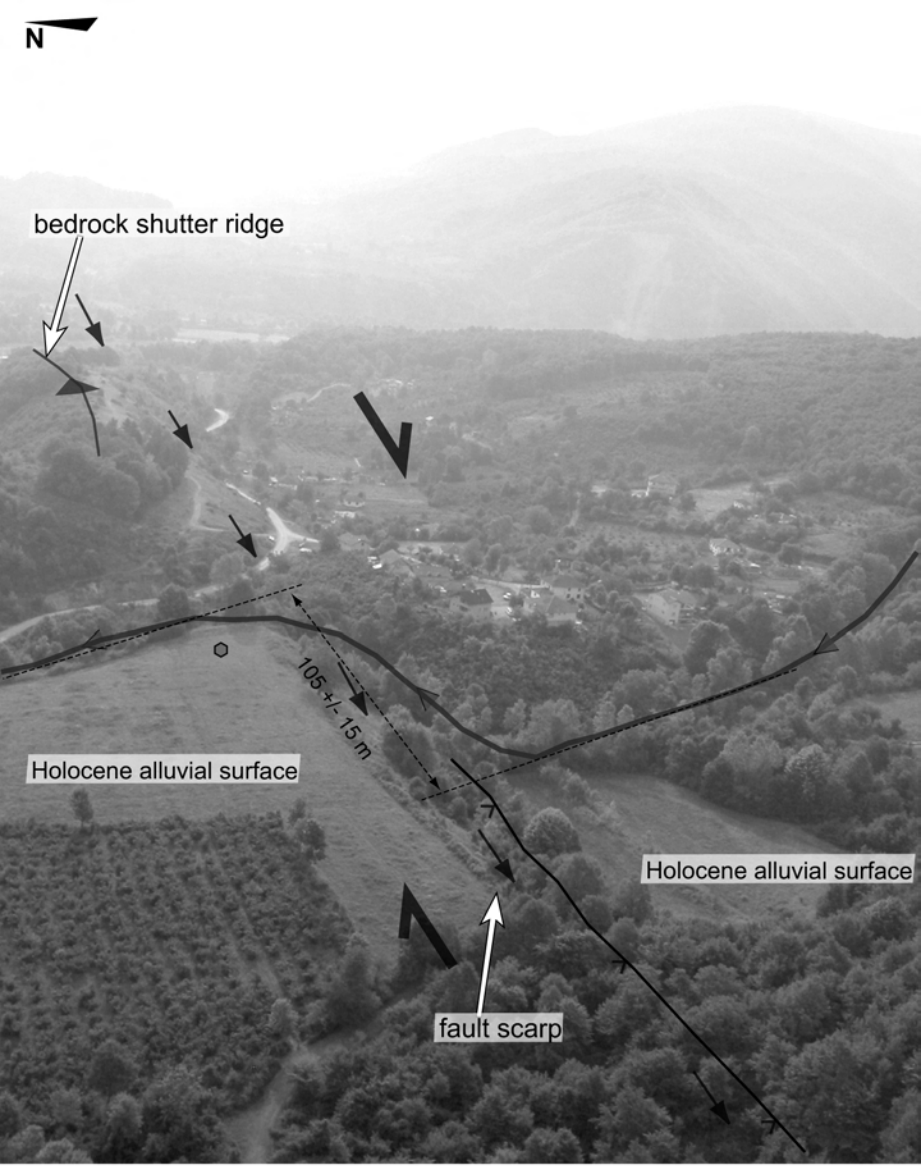
N
bedrock shutter ridge
105 +/- 15 m
Holocene alluvial surface
Holocene alluvial surface
fault scarp

Fig. 6

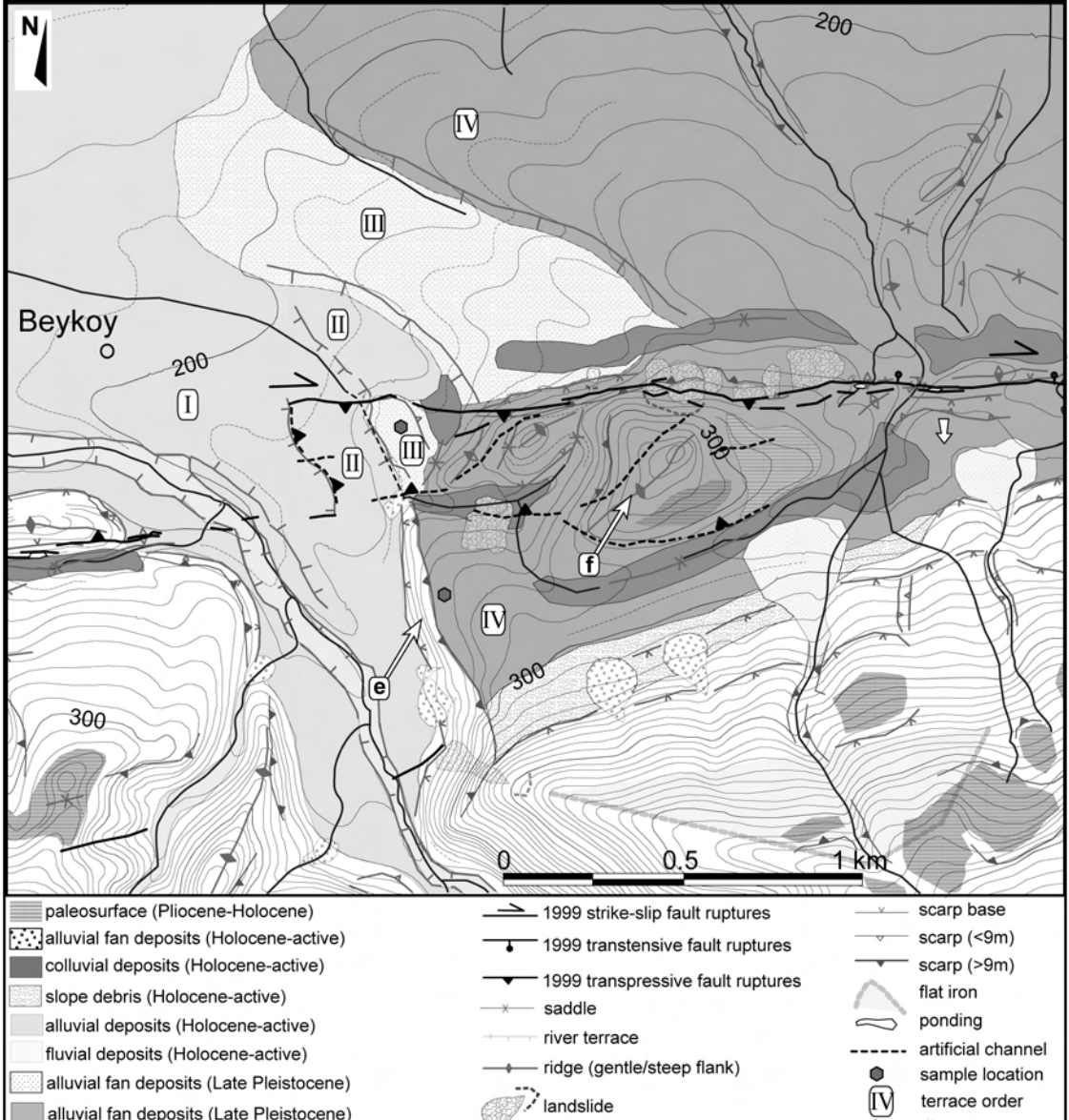
N
Beykoy
200
300
I
II
III
IV
e
f
0
0.5
1 km
paleosurface (Pliocene-Holocene)
alluvial fan deposits (Holocene-active)
colluvial deposits (Holocene-active)
slope debris (Holocene-active)
alluvial deposits (Holocene-active)
fluvial deposits (Holocene-active)
alluvial fan deposits (Late Pleistocene)
alluvial fan deposits (Late Pleistocene)
1999 strike-slip fault ruptures
1999 transtensive fault ruptures
1999 transpressive fault ruptures
saddle
river terrace
ridge (gentle/steep flank)
landslide
scarp base
scarp (<9m)
scarp (>9m)
flat iron
ponding
artificial channel
sample location
terrace order
tilt

Fig. 7

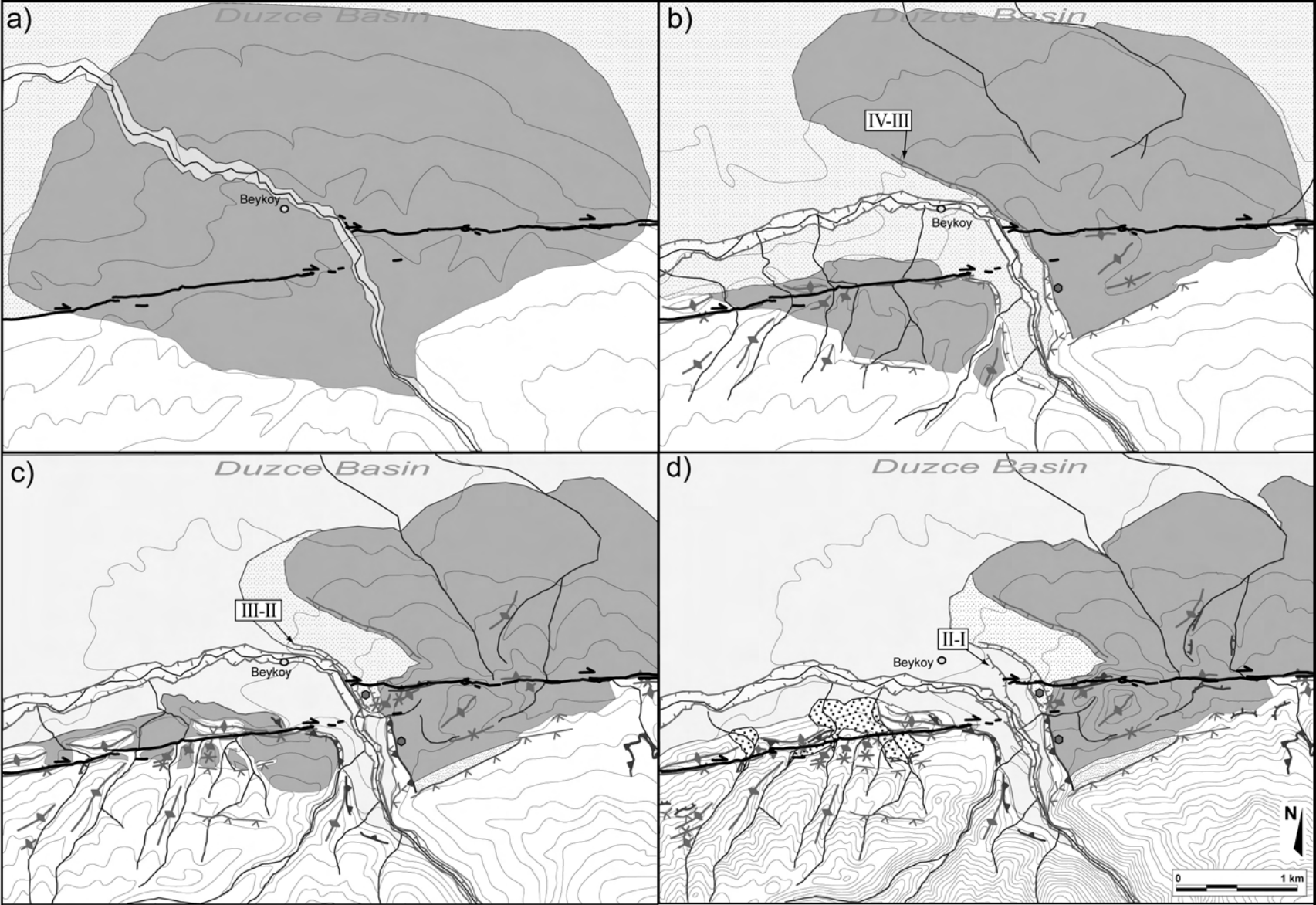
a)
Duzce Basin
Beykoy
b)
Duzce Basin
IV-III
Beykoy
c)
Duzce Basin
III-II
Beykoy
d)
Duzce Basin
II-I
Beykoy
N
0
1 km
slope debris (Holocene-active)
alluvial deposits (Holocene-active)
alluvial fan deposits (Holocene)
alluvial fan deposits (Pleistocene)
alluvial fan deposits (Pleistocene)
1999 ruptures
saddle
river terrace
ridge
scarp base
scarp (<9m)
scarp (>9m)
II-I terrace riser
sample location

Fig. 8

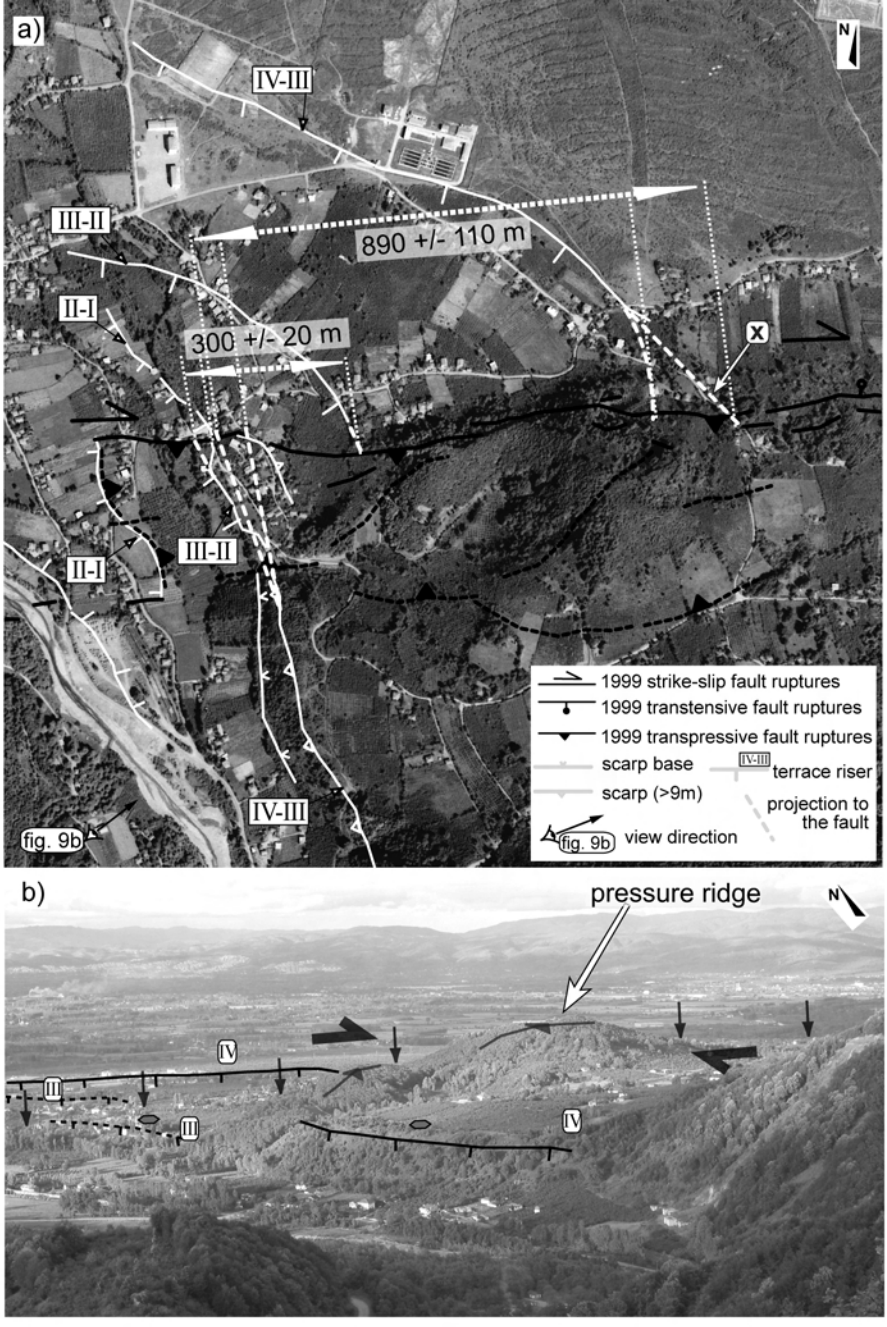
a)
N
IV-III
III-II
890 +/- 110 m
II-I
300 +/- 20 m
X
III-II
II-I
IV-III
fig. 9b
1999 strike-slip fault ruptures
1999 transtensive fault ruptures
1999 transpressive fault ruptures
scarp base
IV-III
terrace riser
scarp (>9m)
projection to the fault
fig. 9b
view direction
b)
pressure ridge
N
IV
III
III
IV

Fig. 9

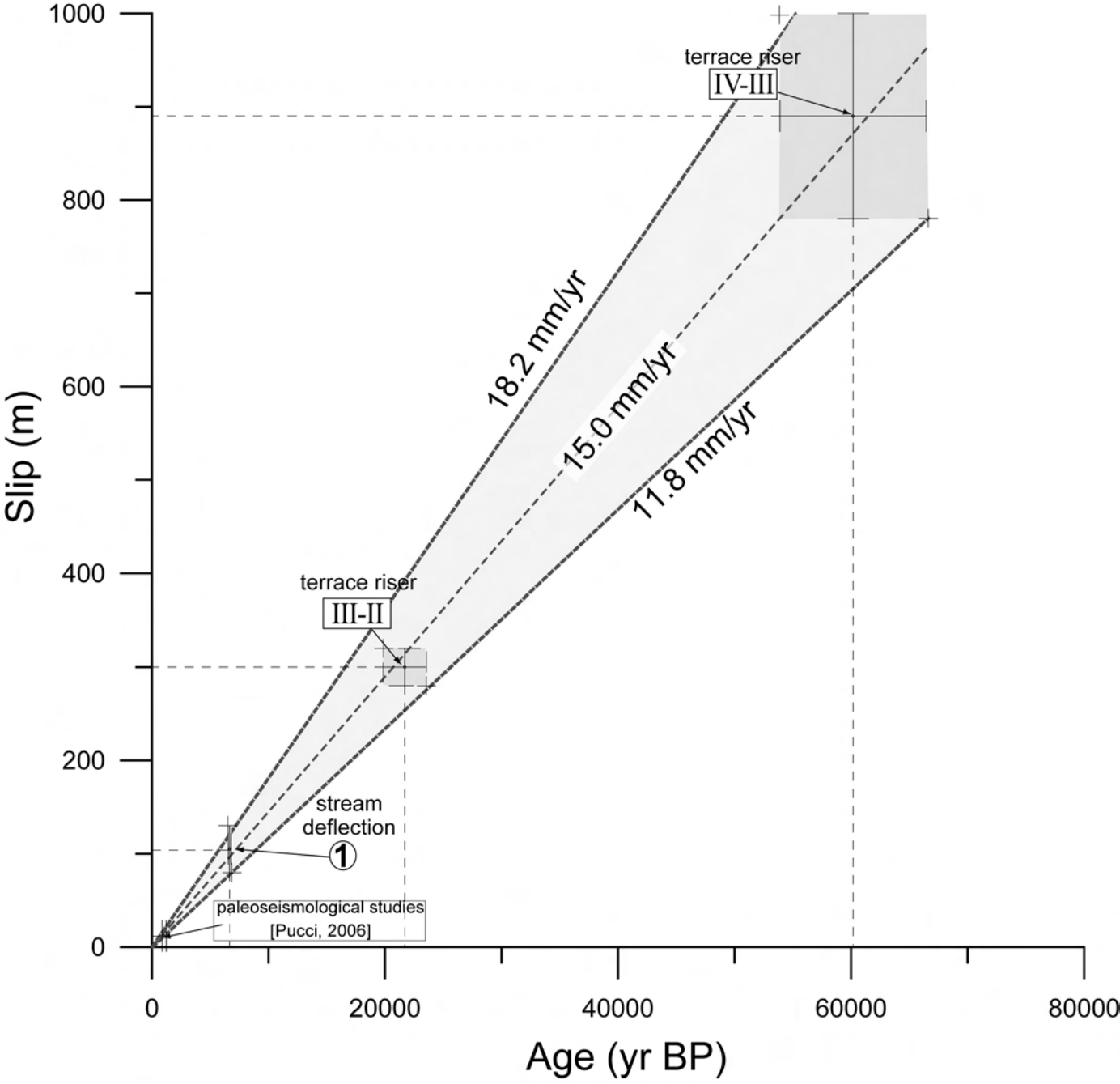
terrace riser
IV-III
18.2 mm/yr
15.0 mm/yr
11.8 mm/yr
terrace riser
III-II
stream
deflection
1
paleoseismological studies
[Pucci, 2006]
Slip (m)
Age (yr BP)
0
200
400
600
800
1000
0
20000
40000
60000
80000

Fig. 10